LAWRENCE
LIVERMORE
NATIONAL
LABORATORY

LLNL-PROC-658263

Nitrogen Oxides as a Chemistry Trap in Detonating Oxygen-Rich Materials

N. Goldman, S. Bastea

August 5, 2014

15th International Detonation Symposium
San Francisco, CA, United States
July 13, 2014 through July 18, 2014

Disclaimer

Nitrogen Oxides as a Chemistry Trap in Detonating Oxygen-Rich Materials

Nir Goldman and Sorin Bastea

Physical and Life Sciences Directorate, Lawrence Livermore National Laboratory

Abstract. Despite decades of research, the chemical processes and states of matter that govern the behavior of energetic materials under detonation conditions are not well understood, including the molecular level processes that determine decomposition kinetics and energy release. Oxygen content is often employed as a simple and intuitive guide to the development and practical use of explosives, but its effect on detonation chemistry remains little studied, especially for the case of oxygen overabundance. To this end, we have conducted quantum molecular dynamics (QMD) simulations of zero oxygen balance and oxygen-rich mixtures of hydrogen peroxide and nitromethane under detonation-like conditions to near equilibrium time-scales. We find excellent agreement between our extrapolated chemical equilibrium properties and those from thermochemical models for the zero oxygen balance mixture. In contrast, for the oxygen-rich mixture we observe the formation of nitrogen oxide intermediates, particularly nitrate ions (NO_3), that effectively act as an oxygen/nitrogen "trap" by precluding the formation of the equilibrium products N_2 and CO_2. Our results could have implications for the design and modeling of oxygen-rich energetics in common military and industrial use.

Explosive materials generally contain both oxidizing (oxygen-rich) and reducing (oxygen-poor) groups, which under the high pressure and temperature conditions typical of a detonation shock wave produce small gaseous products with low heats of formation, such as H_2O, N_2, CO and CO_2[1]. Despite their extensive production and practical use for numerous industrial and military applications[2], the basic microscopic properties for many energetic materials during shock-induced chemical decomposition are not well known. Detonation wave reaction times (i.e., steady-state reaction zones lengths) are inferred from hydrodynamic measurements to be anywhere between nanosecond to microsecond time scales[3]. However, the molecular level processes that govern the extent of the reaction zone are poorly understood for many organic materials and composites, with longer time scale kinetics (e.g., larger than a few nanoseconds) frequently thought to result in carbon-rich, oxygen-poor explosives from processes such as carbon condensation and coagulation[4], possibly coupled with slow CO_2 formation.

The oxygen balance (degree to which an explosive can be oxidized) is known to correlate well with both performance[5] and sensitivity properties[6], and therefore it is an important metric for the synthesis of new energetic compounds[7, 8]. A convenient avenue for controlling oxygen balance in energetic mixtures is to combine oxygen-rich and oxygen-poor materials, as done for example in the widely used ammonium nitrate-fuel oil (ANFO) formula-

tion [9]. These types of mixtures have widespread use in mining and civil construction due to their low cost and relative insensitivity. However, oxygen-rich mixtures tend to exhibit large reaction zones, which result in high failure diameters (i.e., the minimum charge diameter at which propagation of a steady detonation is possible)[10] and poor performance. The development and use of high performance oxidizers and their mixtures remain of much interest for a variety of applications, including civil engineering, rocket propellants, and munitions[11], which would directly benefit from a fundamental understanding of their chemical reactivity at extreme conditions such as those encountered during detonation.

Molecular dynamics (MD) simulations provide an independent route to chemical speciation that occurs during detonation-like conditions, which could facilitate future design and use of energetic materials. Accurate modeling of the breaking and formation of chemical bonds behind a shock front frequently requires the use of a quantum theory[12, 13], such as density functional tight binding[14] (DFTB). DFTB (with self-consistent atomic charges; SCC) is an approximate quantum simulation technique that allows for several orders of magnitude increase in computational efficiency while retaining most of the accuracy of standard quantum simulations, (e.g., Kohn-Sham Density Functional Theory; DFT[15]). This allows DFTB simulations to achieve close to equilibrium timescales for long-timescale reactivity (e.g., several hundred picoseconds or greater[13]), whereas DFT-MD calculations are generally limited to tens of picoseconds[16] and can be far from equilibrium under similar conditions[12]. DFTB has been shown to provide accurate descriptions of chemical reactivity for number of systems under extreme conditions, including nitromethane[17] and other organic materials[18, 19, 20]. Recently, DFTB was used to validate both the equation of state and decomposition kinetics of hydrogen peroxide (H_2O_2) under detonation conditions from picosecond time-resolved shock compression experiments[21].

In this work, we predict an entirely new mechanism for the slow chemical reactivity of nitrogen-containing, oxygen-balanced to oxygen-rich explosive mixtures under detonation conditions using the DFTB quantum simulation method. We focus on liquid explosives and choose hydrogen peroxide and nitromethane as prototypical energetic materials with an excess and deficit of oxygen, respectively. Our simulations consisted of 60/40 molar ratio (zero oxygen balance) and 80/20 molar ratio (positive oxygen balance) mixtures of hydrogen peroxide/nitromethane under detonation-like conditions. (Zero oxygen balance corresponds to a mixture with exactly enough oxygen to turn all carbon into CO_2 and all hydrogen into H_2O; positive oxygen balance corresponds to a system with a surfeit of oxygen [5].). We first validate our results for the thermodynamic properties of each mixture against results from equation of state (EOS) chemical equilibrium models[22]. We then analyze the long timescale chemical reactivity of both mixtures and find that the rate of formation of the end products CO_2 and especially N_2 is determined in part by the slow kinetics from nitrogen oxide intermediates. This leads to the striking result in the oxygen-rich mixture that nitrate (NO_3) acts as a major nitrogen and oxygen "trap", leading to a very long-lived, likely metastable thermodynamic state. Our results can help elucidate the properties of these types of materials under extreme conditions, including the reaction zones, and could be useful in guiding their effective use.

Computational Methods

Direct chemical equilibrium calculations were performed for these mixtures using the methodology outlined in Ref.[22]. In these calculations the individual molecular products are modeled by exp6-polar interactions parameterized by a wide range of experimental data (e.g. static and dynamic pressure experiments, sound speed measurements), and the system thermodynamics is derived using statistical mechanics techniques. This approach has proved to be successful for predicting the properties of a variety of reactive materials at high pressures and temperatures, including shock Hugoniots and detonation velocities[23].

DFTB-SCC calculations were driven by the LAMMPS molecular software simulation suite[24], with the DFTB+ code[25] used to compute forces and the cell stress tensor. We used C-H-O-N interaction parameters available for download (mio-0-1 parameter set from http://www.dftb.org). The maxi-

mum number of SCC steps for each MD time step was reduced to four through use of the Extended Lagrangian Born-Oppenheimer molecular dynamics (XL-BOMD) approach for propagation of the electronic degrees of freedom[26]. Thermal populations of excited electronic states are computed through the Mermin functional[27]. All simulations discussed here were performed with a time-step of 0.2 fs. The zero oxygen balance mixture was set up with 36 H_2O_2 and 24 CH_3NO_2 molecules (312 atoms total). Zero pressure optimization produced computational-cell lattice vectors of $a = 23.9961$ Å, $b = 11.9980$ Å, and $c = 11.9980$ Å, yielding an in initial density of 1.29 g/cc, compared to the EOS computed value of 1.26 g/cc. The positive oxygen balance mixture contained 72 H_2O_2 and 12 CH_3NO_2 molecules (276 atoms). This was optimized to lattice vectors of $a = 22.7646$ Å, $b = 11.3823$ Å, and $c = 11.3823$ Å, yielding an initial density of 1.33 g/cc, the same as the EOS computed value. Each initial mixture was equilibrated at 300 K for 10 ps using Nose-Hoover thermostat chains[28, 29]. Uniaxial compression due to the shock wave occurred along the a lattice vector. Previous work has shown that doubling the system size along the a lattice vector for a similar system and size yielded virtually identical thermodynamic conditions under shock loading[12].

Shock compression simulations were conducted using the well-established Multi-scale Shock compression Simulation Technique (MSST)[30]. MSST operates by time-evolving equations of motion for the atoms and the computational cell dimension in the direction of the shock to constrain the stress in the propagation direction to the Rayleigh line and the energy of the system to the Hugoniot energy condition. For a given shock speed, these two relations describe a steady planar shock wave within continuum theory. MSST has been used in conjunction with quantum simulation methods to accurately reproduce the shock Hugoniot of a number of systems (e.g., , Ref.[21]). For all shock velocities we used a scaling term with the MSST ionic equations of motion to account for drift in the conserved quantity in our simulations[13]. A scaling factor of 10^{-4} resulted in a deviation in the total forces in our simulations of less than 1% once a steady shock compression had been produced. Simulations were run for up to 40 ps, excluding those near detonation conditions, which were allowed to evolve for up to 250 ps within the shock state. The deviation from the Hugoniot energy and Rayleigh line conditions for all of our shock compression simulations was less than 1%.

Results and Discussion

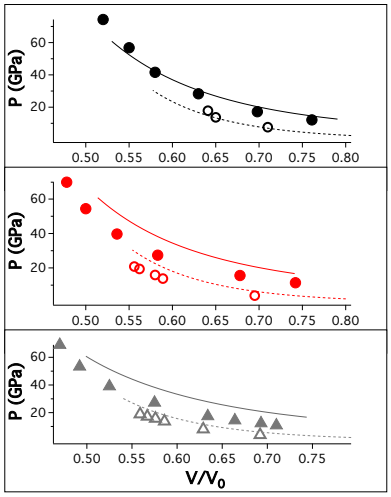

Fig. 1. Pressure vs. relative volume Hugoniot curves for pure H_2O_2 (black), positive oxygen balance (red), and zero oxygen balance mixtures (gray). The dashed and solid lines corresponds to EOS results for the unreacted and reacted Hugoniot, respectively, and the open and closed circles to the same from DFTB. DFTB simulations of the positive and zero oxygen balance mixtures are slow to reach equilibrium on the time scales of our simulations.

For both mixtures, we simulated shock velocities between 3 – 10 km/s, spanning pressures of 4 – 70 GPa and compressions of 1.43 – 2.13 times the initial density. The Hugoniot temperatures of the zero oxygen balance mixture spanned 450 – 5670 K, and the positive oxygen balance mixture from 440 – 5790 K. For simulations that were over-driven, the system achieved a reactive state within 5 ps of compression. Comparison of our computed pressure vs. density Hugoniot results show good agreement with

EOS calculations (Fig. 1). We observe excellent agreement for systems of pure peroxide for both the unreacted and reacted Hugoniot curves, in part due to the rapid chemical equilibrium of H_2O_2 under shock loading[21]. The agreement for the zero and positive oxygen balance mixtures is reasonable for the unreacted Hugoniot, though somewhat worse for the reacted curve. This is likely due primarily to the slow reactivity of the system, where chemical equilibrium and the concurrent expansion have not been achieved on the timescales of our simulations. Chemical equilibrium calculations [22] yield detonation velocities of 6.93 km/s for the zero oxygen balance mixture and 6.75 km/s for the positive oxygen balance mixtures. Here, we analyze the equation of state and ensuing chemistry of both mixtures at 7 km/s. Slightly overdriven conditions avoid any possible instability in the MSST method below detonation conditions[31] and allow for faster chemical reactivity that is more readily modeled on the timescales of the present simulations.

We determine the specific chemical reactivity in our simulations using a pre-established methodology of optimal bond cutoff distances and lifetimes[13]. The optimal value for r_c to distinguish between bonded and nonbonded atomic sites is given by the first minimum in the corresponding pair radial distribution function $g(R)$, which corresponds to the maximum of the potential of mean force, viz., $W(R) = -k_B T \ln[g(R)]$, for all possible bonding pairs. In addition, in order to avoid counting species that were entirely transient and not chemically bonded, we also chose a lifetime cutoff τ_c of 20 femtoseconds for C-H, O-H, and N-H bonds and 50 femtoseconds for all others (N.B., no H-H bonds were detected in any of our simulations). This criteria is intuitive since bonds with this lifetime could conceivably be detected spectroscopically. As a result, atom pairs were considered to be bonded only if they resided within a distance of each other of r_c for a time of greater than τ_c. The concentrations of species at high pressure and temperature have some dependence on bond and lifetime criteria, as expected and has been shown for other hot dense materials[12]. We found that the overall conclusions of this work were independent of these parameters.

Time traces of the equation of state properties

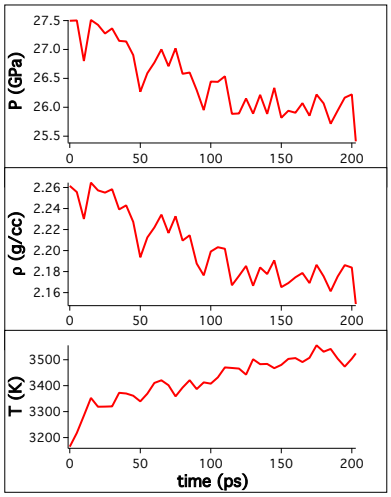

Fig. 2. Pressure, density, and temperature time traces for the zero oxygen balanced mixture during shock compression at close to detonation conditions. The time coordinate is shifted so that $t = 0$ corresponds to the onset of shock compression, and results are averaged over 5 ps windows.

of the zero oxygen balance mixture indicate that the system has not yet achieved thermodynamic equilibrium, though chemistry-induced expansion is observable on the timescales of the simulations (Fig. 2). The sudden increase in temperature and pressure due to shock loading leads to the synthesis of a number of detonation products, including H_2O, N_2, CO_2, CO (Fig. 3). We also observe significant amounts of the nitrogen oxide compounds NO (nitric oxide), NO_2 (nitrogen dioxide), and the nitrate ion NO_3 (i.e., dissociated nitric acid, HNO_3). Nitrogen oxides are commonly formed during combustion of nitrogen-containing fuels[32]. We find that the concentrations of NO molecules are approximately 5-6 times those of NO_3 and NO_2, respectively, throughout the course of this simulation. The decomposition of H_2O_2 occurs according to the expected mechanism of $2H_2O_2 \rightarrow 2H_2O + O_2$, with H_2O subsequently reacting with the methyl group in CH_3NO_2 to form formic acid (HCOOH) and carbonic acid (H_2CO_3) intermediates. CO and CO_2 are then produced through elimination of a water molecule from each intermediate, respectively.

H_2O has been shown to catalyze the formation of C-O bonded compounds in carbon-rich explosives under detonation conditions[33]. We also observe that after shock compression, approximately 11% of the number of reactions yielding CO_2 as a product occur through oxidation of CO, which may be the main mechanism for evolution of CO towards its chemical equilibrium concentration.

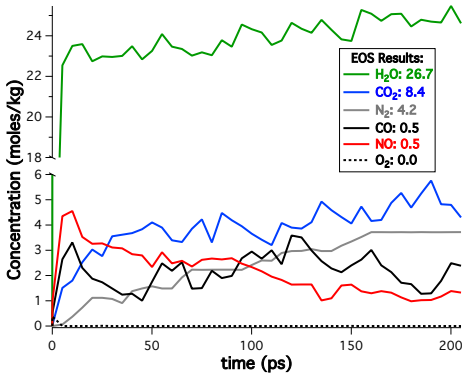

Fig. 3. Time traces for the zero oxygen balance mixture of the major chemical species, compared to EOS results (figure legend). Results labeled 'NO' from our MD simulations correspond to concentrations of NO, NO_2, and NO_3 summed together. Due to its short molecular lifetimes, results labeled 'H_2O' from our MD simulations correspond to H_2O and OH concentrations summed together. All concentration time traces have non-zero slopes, indicating that the system is progressing to chemical equilibrium over the time scale of our simulation.

Molecular nitrogen synthesis occurs through the following four step sequence: (1) reduction of NO_2 from nitromethane by a hydrogen ion from dissociated water: $NO_2 + H \rightarrow NO + OH$; (2) dimerization of NO molecules: $NO + NO \rightarrow (NO)_2$; (3) reduction of the NO dimer (hyponitrite) by an additional hydrogen ion: $(NO)_2 + H \rightarrow N_2O + OH$; (4) elimination of an oxygen ion from an N_2O molecule: $N_2O \rightarrow N_2 + O$. For this system, the relatively high NO concentration is a key aspect of N_2 formation. $(NO)_2$ has been observed in low temperature gas phase[34] and condensed phase studies[35], and is known to lead to N_2 formation via an N_2O intermediate in catalytic systems[36]. In this case, the need for a catalyst is obviated by the extreme pressures and temperatures, and the presence of reducing agents such as CO and hydrogen ions. For both carbon and nitrogen oxide formation, water from the peroxide decomposition is observed to play a crucial role, either as catalyst or intermediate reactant. Lifetimes of the majority products (Table 1) indicate that N_2 (14 ps), CO (2 ps), and N_2O (2 ps) have relatively long lifetimes, compared to the hundreds of fs values for all other listed species. We note that short lifetimes are due in part to fleeting interactions with H and OH from dissociated water, which results in the formation of many transient species (e.g., HCO_2) with computed lifetimes of hundreds of femtoseconds and below.

Table 1. Average lifetimes of chemical products for the zero oxygen balance mixture.

Compound	Lifetime (ps)
H_2O	0.237
CO_2	0.551
N_2	13.804
CO	1.880
NO	0.619
NO_2	0.122
NO_3	0.186
N_2O	2.177

Given the short chemical lifetimes and complex reactivity in our simulations, we have generalized chemical events by examining the time traces of concentrations of specific bond types (Fig. 4). This allows for a detailed chemical picture under these conditions without relying on the fate of specific compounds and any intermediates they might form. We observe that concentrations of O-X (X=C, N, O, H) and N-N bonds all appear to be approaching equilibrium on the timescales of our simulations. In order to estimate their equilibrium values, we first shift the time origin to the onset of shock compression (where the temperature becomes relatively constant) and fit each time trace to a simple exponential form. Specifically, the time-dependent bond concentrations $C(t)$ of O-C, O-H, and N-N bonds were fit to a function of the form $C(t) =$

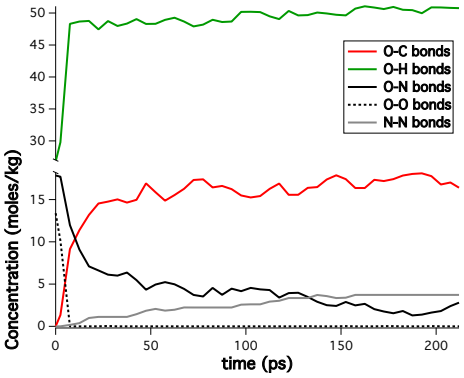

Fig. 4. Time traces for the zero oxygen balance mixture of O-H bonds (e.g., H_2O), O-C bonds (e.g., CO, CO_2), O-N bonds (e.g, NO, NO_2, and NO_3), O-O bonds (e.g., O_2), and N-N bonds (e.g., N_2). O-O bonds disappear after ∼15 ps, whereas, O-H, O-C, O-N and N-N bonds all exhibit slow chemistry over these timescales.

$A_1(1-e^{-kt})+A_2$, with the equilibrium values estimated by A_1+A_2, and the O-N bond concentration trace was fit to $C(t) = A_1e^{-kt} + A_2$, with the estimated the equilibrium value equal to A_2. This type of analysis provides a straightforward method for making comparisons to chemical equilibrium calculations. The resulting time constants k^{-1} range from ∼20 ps for the for O-C bonds to ∼300 ps for O-H bonds. This implies that chemical equilibrium for this system is achieved over timescales of hundreds of picoseconds to nanoseconds. We find that our computed equilibrium concentrations of O-X and N-N bonds agree well with those determined from the EOS equilibrium chemistry (Table 2). In particular, we see close agreement for O-C, O-O, O-H, and N-N bond concentrations, which provides good validation for the equilibrium chemistry predicted by the mio-0-1 parameter set under these extreme thermodynamic conditions. The extrapolated value for the O-N equilibrium concentration is somewhat higher than the EOS value in part due to the fact that our simulations predict some amount of NO_2 and NO_3, whereas the chemical equilibrium calculation finds NO as the main nitrogen oxide molecule. Charged products like NO_3 are also traditionally not included in chemical equilibrium calculations, although such modeling may be within reach [37].

Table 2. Equilibrium concentrations of different bond types chemical products for the zero oxygen balance mixture. Concentrations are shown in units of moles/kg. DFTB results are extrapolated by fitting to exponential functional forms.

Bond type	DFTB	EOS
O-H	53.4	53.4
C-O	16.7	17.3
O-N	2.0	0.5
N-N	4.5	4.2
O-O	0.0	0.0

In contrast, equation of state results for the oxygen rich mixture indicate much less variation after shock compression (Fig. 5). The pressure, density, and temperature time traces all appear to oscillate about a mean value, rather than indicating a chemistry-induced expansion. We observe H_2O, CO_2, CO, O_2, and nitrogen oxides as detonation products, all of which appear to be in a quasi-steady chemical state (Fig. 6). In this case the NO_3 ion is the dominant nitrogen oxide product by far, with a concentration that is approximately three times that of both NO and NO_2. The concentrations of H_2O, nitrogen oxides, and CO_2 all vary only slightly over the timescale of this simulation, and the quasi-steady values for CO_2 and nitrogen oxide compounds are all somewhat lower than the EOS model predictions. In addition, we observe only trace amounts of O_2 and CO, and zero N_2 production, in contrast to the values of 5.5, 5.1, and 1.7 moles/kg, respectively, predicted by the chemical equilibrium calculation. This seemingly slow equilibrium chemistry relative to the zero oxygen balance mixture is surprising given the enhanced chemical reactivity, where the average lifetimes predicted for the major detonation products are all under 500 fs (Table 3). In particular, we note that the computed lifetime for H_2O is roughly half the value and that of CO his approximately one order of magnitude smaller than their corresponding values in the zero oxygen balance mixture. This is in part due to the higher mole fraction of H_2O_2 starting material,

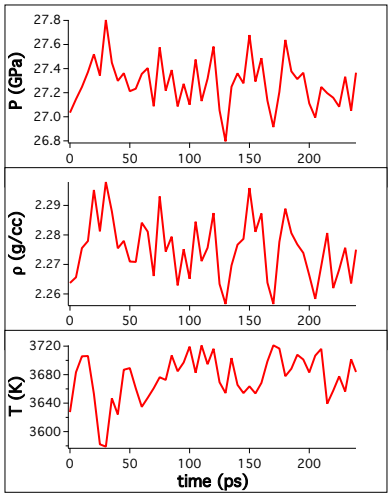

Fig. 5. Pressure, density, and temperature time traces for the positive oxygen balanced mixture during shock compression at close to detonation conditions. The time coordinate is shifted so that $t = 0$ corresponds to the onset of shock compression, and properties are averaged over 5 ps windows.

which yields higher concentrations of H and OH ions (due to water dissociation), which in turn promotes reactivity with other chemical species (e.g., $CO + H + OH \rightarrow HCOOH$).

Analysis of the reaction mechanisms in the shock compressed mixture indicate that CO and CO_2 also largely form through the elimination of water from formic and carbonic acids. Similar to the zero oxygen balance mixture, approximately 12% of the number of CO_2 forming reactions occur though oxidation of CO molecules. The nitrogen oxide chemistry is dominated by the direct oxidation of nitric oxide and NO_2 to NO_3, as well as protonation/deprotonation reactions involving NO_3/HNO_3. In part due to both steric hindrance and its overall charge, the NO_3 ions have increased difficulty in dimerizing. This in effect traps some of the supply of both the nitrogen and oxygen atoms into a metastable product, directly inhibiting the formation of N_2 and the release of oxygen to form O_2 and CO_2. We observe some $(NO_3)_2$ formation in our simulation, though the product is short-lived ($\sim$ 60 fs) and its formation is almost entirely balanced by its dissociation into monomers. This "trapping" of the chemistry is clearly seen in the time traces of the bond type concentrations (Fig. 7), where the values for O-H, O-C, and O-N bonds remain flat over these timescales, O-O bonds hover slightly above zero concentration, and N-N bonds are not formed at all during our simulations. This indicates a mechanism where CO_2 and N_2 equilibrium will likely be achieved on significantly longer timescales than the zero oxygen balance mixture, due in part to the higher oxygen content and lower nitric oxide concentration in the detonation products.

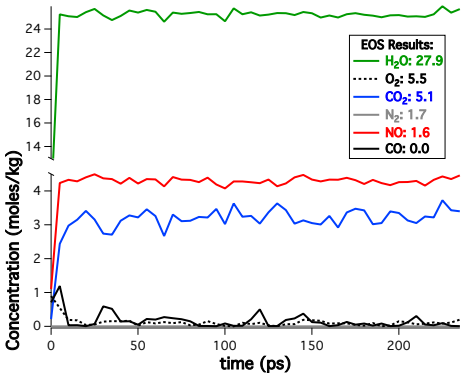

Fig. 6. Time traces for the positive oxygen balance mixture of the major chemical species, compared to EOS results (figure legend). Similar to 2, results labeled 'NO' correspond to concentrations of NO, NO_2, and NO_3 summed together and those labeled 'H_2O' to concentrations of H_2O and OH summed together.

Conclusions

Our results indicate a new model for reaction zone kinetics in oxygen-rich to oxygen balanced energetic materials that is governed by the relatively slow chemical reactivity of nitrogen oxide compounds in a process reminiscent of combustion. For the oxygen balanced mixture, molecular nitrogen synthesis is driven through the dimerization of NO molecules and the formation of the N_2O intermediate; concomitantly, the oxidation of CO to CO_2 moves the system towards the expected chemical equilibrium state. The oxygen rich

Table 3. Average lifetimes of chemical products for the positive oxygen balance mixture. N_2 molecules were not detected on the time scales of our simulations.

Compound	Lifetime (ps)
H_2O	0.129
CO_2	0.341
CO	0.232
NO	0.449
NO_2	0.127
NO_3	0.143
O_2	0.112

mixture on the other hand yields a relative abundance of nitrate ion (NO_3) intermediate, which inhibits nitrogen oxide dimer formation and subsequent N_2 release. As a result, NO_3 ion formation effectively leads to the trapping of the system in a likely metastable, zero N_2 production state that slows down further chemical energy release. This is in sharp contrast to the decomposition mechanism of negative oxygen balance energetic materials (e.g., PETN and TATB), where N-O chemistry equilibrates extremely rapidly, and carbon condensation/coagulation and carbon-oxygen bond chemistry are the rate limiting steps to achieving chemical equilibrium[33]. These results could have significant implications for oxygen-rich energetics, where the detonation chemistry time scales could be larger than usually assumed, and slow nitrogen oxide kinetics could be a significant factor in the poor performance of these materials[38, 39]. Further work is underway to fully characterize the N-O chemistry under these conditions for possible use in continuum scale reactive-flow models.

Acknowledgments

This work was performed under the auspices of the U.S. Department of Energy by Lawrence Livermore National Laboratory (LLNL) under Contract DE-AC52-07NA27344. The project 11-ERD-067 was funded by the Laboratory Directed Research and Development Program at LLNL with S. B. as principal investigator.

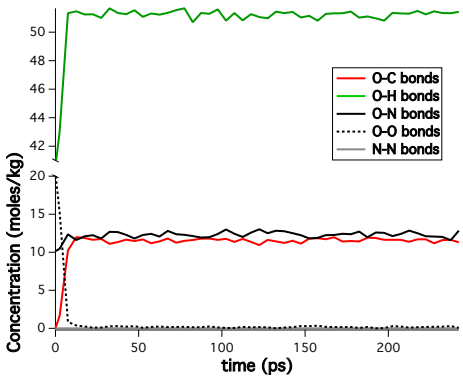

Fig. 7. Time traces for the positive oxygen balance mixture of O-H bonds, O-C bonds, O-N bonds, O-O bonds, and N-N bonds. The system has achieved a metastable kinetic state shortly after the onset of shock compression

References

1. Ornellas, D. L., "The heat and products of detonation in a calorimeter of CNO, HNO, CHNF, CHNO, CHNOF, and CHNOS explosives," *Combustion and Flame*, Vol. 23, pp. 37 – 46, 1974.

2. Meyer, R., Köhler, J. and Homburg, A., *Explosives*, Wiley-VCH Verlag GmbH, Weinheim, 6th edition, 2007.

3. Manaa, M. R., Reed, E. J., Fried, L. E. and Goldman, N., "Nitrogen-Rich Heterocycles as Reactivity Retardants in Shocked Insensitive Explosives," *J. Am. Chem. Soc.*, Vol. 131, p. 5493, 2009.

4. Bastea, S., "Aggregation kinetics of detonation nanocarbon," *Appl. Phys. Lett.*, Vol. 100, p. 214106, 2012.

5. Martin, A. R. and Yallop, H. J., "Some aspects of detonation. Part 2.-Detonation velocity as a function of oxygen balance and heat of formation," *Trans. Faraday Soc.*, Vol. 54, pp. 264–267, 1958.

6. Kamlet, M. J. and Adolph, H. G., "The relationship of Impact Sensitivity with Structure of

Organic High Explosives. II. Polynitroaromatic explosives," *Propellants, Explosives, Pyrotechnics*, Vol. 4, pp. 30–34, 1979.

7. Pagoria, P. F., Lee, G. S., Mitchell, A. R. and Schmidt, R. D., "A review of energetic materials synthesis," *Thermochimica Acta*, Vol. 384, pp. 187 – 204, 2002.

8. Thottempudi, V., Forohor, F., Parrish, D. A. and Shreeve, J. M., "Tris(triazolo)benzene and Its Derivatives: High-Density Energetic Materials," *Angewandte Chemie International Edition*, Vol. 51, pp. 9881–9885, 2012.

9. Hopler, R. B., editor, *Blasters Handbook*, ISEE, 17th edition, 1998.

10. Catanach, R. A. and Hill, L. G., "Diameter Effect Curve and Detonation Front Curvature Measurements for ANFO," *AIP Conference Proceedings*, Vol. 620, pp. 906–909, 2002.

11. Badgujara, D. M., Talawarb, M., Asthanab, S. and Mahulikara, P., "Advances in science and technology of modern energetic materials: An overview," *Journal of Hazardous Materials*, Vol. 151, p. 289, 2008.

12. Goldman, N., Reed, E. J., Fried, L. E., Kuo, I.-F. W. and Maiti, A., "Synthesis of glycine-containing complexes in impacts of comets on early Earth," *Nat. Chem.*, Vol. 2, p. 949, 2010.

13. Goldman, N. and Tamblyn, I., "Prebiotic Chemistry within a Simple Impacting Icy Mixture," *The Journal of Physical Chemistry A*, Vol. 117, pp. 5124 – 5131, 2013.

14. Elstner, M., Porezag, D., Jungnickel, G., Elsner, J., Haugk, M., Frauenheim, T., Suhai, S. and Seifert, G., "Self-consistent-charge density-functional tight-binding method for simulations of complex materials properties," *Phys. Rev. B*, Vol. 58, p. 7260, 1998.

15. Kohn, W. and Sham, L., "Self-consistent equations including exchange and correlation effects," *Phys. Rev. A*, Vol. 140, p. 1133, 1965.

16. Goldman, N., Reed, E. J. and Fried, L. E., "Quantum Corrections to Shock Hugoniot Temperatures," *J. Chem. Phys.*, Vol. 131, p. 204103, 2009.

17. Reed, E. J., Manaa, M. R., Fried, L. E., Glaesemann, K. R. and Joannopoulos, J. D., "A Transient Semi-Metallic Layer in Detonating Nitromethane," *Nature Physics*, Vol. 4, pp. 72–76, 2008.

18. Margetis, D., Kaxiras, E., Elstner, M., Frauenheim, T. and Manaa, M. R., "Electronic structure of solid nitromethane: Effects of high pressure and molecular vacancies," *J. Chem. Phys.*, Vol. 117, p. 788, 2002.

19. Qi, T., Bauschlicher, C. W., Lawson, J. W., Desai, T. G. and Reed, E. J., "Comparison of ReaxFF, DFTB, and DFT for Phenolic Pyrolysis. 1. Molecular Dynamics Simulations," *The Journal of Physical Chemistry A*, Vol. 117, pp. 11115–11125, 2013.

20. Bauschlicher, C. W., Qi, T., Reed, E. J., Lenfant, A., Lawson, J. W. and Desai, T. G., "Comparison of ReaxFF, DFTB, and DFT for Phenolic Pyrolysis. 2. Elementary Reaction Paths," *The Journal of Physical Chemistry A*, Vol. 117, pp. 11126–11135, 2013.

21. Armstrong, M. R., Zaug, J. M., Goldman, N., Kuo, I.-F. W., Crowhurst, J. C., Howard, W. M., Carter, J. A., Kashgarian, M., Chesser, J. M., Barbee, T. W. and Bastea, S., "Ultrafast Shock Initiation of Exothermic Chemistry in Hydrogen Peroxide," *J. Phys. Chem. A*, Vol. 117, p. 13051, 2013.

22. Bastea, S. and Fried, L. E., "Chemical Equilibrium Detonation," in "Shock Wave Science and Technology Reference Library," , edited by Zhang, F., Vol. 6, p. 1, Springer, 2012.

23. Bastea, S. and Fried, L. E., "Exp6-polar thermodynamics of dense supercritical water," *J. Chem. Phys.*, Vol. 128, p. 174502, 2008.

24. Plimpton, S., "Fast Parallel Algorithms for Short-Range Molecular Dynamics," *J. Comp. Phys.*, Vol. 117, p. 1, 1995, http://lammps.sandia.gov.

25. Aradi, B., Hourahine, B. and Frauenheim, T., "DFTB+, a sparse matrix-based implementation of the DFTB method," *J. Phys. Chem. A*, Vol. 111, p. 5678, 2007, http://www.dftb-plus.info.

26. Niklasson, A. M. N., Steneteg, P., Odell, A., Bock, N., Challacombe, M., Tymczak, C. J., Holmström, E., Zheng, G. and Weber, V., "Extended Lagrangian Born–Oppenheimer molecular dynamics with dissipation," *J. Chem. Phys.*, Vol. 130, p. 214109, 2009.

27. Mermin, N. D., "Thermal properties of the Inhomogenous Electron Gas," *Phys. Rev.*, Vol. 137, p. 1441, 1965.

28. Nosé, S., "A unified formulation of the constant temperature molecular dynamics method," *Mol. Phys.*, Vol. 52, p. 255, 1984.

29. Hoover, W. G., "Canonical dynamics: Equilibrium phase space distributions," *Phys. Rev. A*, Vol. 31, p. 1695, 1985.

30. Reed, E. J., Fried, L. E. and Joannopoulos, J. D., "A method for tractable dynamical studies of single and double shock compression," *Phys. Rev. Lett.*, Vol. 90, p. 235503, 2003.

31. Reed, E. J., Rodriguez, A. W., Manaa, M. R., Fried, L. E. and Tarver, C. M., "Ultrafast detonation of Hydrazoic Acid (HN_3)," *Phys. Rev. Lett.*, Vol. 109, p. 038301, 2012.

32. Hill, S. C. and Smoot, L. D., "Modeling of nitrogen oxides formation and destruction in combustion systems," *Progress in Energy and Combustion Science*, Vol. 26, p. 417, 2000.

33. Wu, C., Fried, L. E., Yang, L. H., Goldman, N. and Bastea, S., "Catalytic behaviour of dense hot water," *Nat. Chem.*, Vol. 1, p. 57, 2009.

34. Nour, E. M., Chen, L.-H., Strube, M. and Laane, J., "Raman Spectra and Force Constants for the Nitric Oxide Dimer and Its Isotopic Species," *J. Phys. Chem.*, Vol. 88, p. 757, 1984.

35. Fuente, S. A., Fortunato, L. F., Domancich, N., Castellani, N. J. and Ferullo, R. M., "Formation of nitric oxide dimers on MgO-supported gold particles," *Surf. Sci.*, Vol. 606, p. 1948, 2012.

36. Brown, W. A., Gardner, P. and King, D. A., "Very Low Temperature Surface Reaction: N_2O Formation from NO Dimers at 70 to 90 K Very Low Temperature Surface Reaction: N_2O Formation from NO Dimers at 70 to 90 K on Ag 111," *J. Phys. Chem.*, Vol. 99, p. 7065, 1995.

37. Bastea, S., "Thermodynamics and diffusion in size-symmetric and asymmetric dense electrolytes," *J. Chem. Phys.*, Vol. 135, p. 084515, 2011.

38. Brill, T. B., Brush, P. J. and Patil, D. G., "Thermal Decomposition of Energetic Materials 58. Chemistry of Ammonium Nitrate and Ammonium Dinitramide Near the Burning Surface Temperature," *Combustion and Flame*, Vol. 92, pp. 178 – 186, 1993.

39. Ostmark, H., Helte, A., Karlsson, S., Hahma, A. and Edvinsson, H., "Detonation properties and reaction rate modeling of melt cast ammonium dinitramide (ADN)," *Proceedings of the 12th International Detonation Symposium*, p. 775, 2002.